Effect of Kernel Function on Ultrasonic Fan-Beam Tomographic Reconstructions in Gases using Filtered Back Projection

W. M. D. Wright[1] and P. Ingleby[2]

Ultrasonics Research Group, Department of Electrical and Electronic Engineering, University College Cork, National University of Ireland – Cork, IRELAND

E-mail: [1]bill.wright@ucc.ie [2]pauli@rennes.ucc.ie

Abstract -- **An ultrasonic tomographic imaging system has been developed and used to image solid object distributions, temperature variations, and flow velocity fields in air. The system consisted of a pair of novel curved divergent air-coupled electrostatic ultrasonic transducers that were positioned under computer control in a fan-beam geometry as required. A modified filtered back-projection algorithm was used for the reconstruction, and the effect of different kernel filter functions used on the quality of the reconstructed images was investigated.**

I INTRODUCTION

Ultrasonic tomography [1] is widely used in medicine [2] and engineering [3] to produce cross-sectional images of spatial variations in physical properties, using only measurements made at the periphery of the plane of interest. Backscatter or reflection tomographic techniques [4] are used where it is difficult to propagate ultrasound directly through the plane of interest. These techniques utilise the ultrasonic energy deflected back from discontinuities where there is a large mismatch in specific acoustic impedance, for example cracks or defects in solids [5], bubbles in liquids [6], and solid objects in air [7]. Transmission tomography [8] is used where it is relatively easy to propagate ultrasound through the plane of interest, and utilises the ultrasonic energy that has travelled directly between source and receiver. This technique is sensitive to slight variations in specific acoustic impedance and hence acoustic velocity and density changes in the medium.

Tomographic cross-sectional images may be produced using one of two main types of reconstruction algorithm. Series or expansion methods such as ART [9] and SIRT [10] use iterative techniques, and effectively pixelize the area to be imaged. An initial weighted property value is assigned to each pixel. These values are then modified in successive iterations until a solution is reached. These techniques can account for non-linear effects such as ray-bending and anisotropy, but are computationally inefficient and the reconstruction times are relatively long. Fourier transform methods [11] require a well defined, regular sampling geometry in either a parallel-beam or fan-beam configuration [12], but are quicker to implement than iterative techniques. Essentially, datasets taken at different angles through the area to be imaged are multiplied by a kernel function in the Fourier domain, and then back-projected to give the reconstructed cross-sectional image. The type of kernel function used has a significant effect on the accuracy of the reconstruction and the quality of the image obtained.

Little attention has been paid to tomographic imaging of gaseous media [13]. This is due in no small part, until recently, to the lack of suitable ultrasonic transducers capable of generating and detecting broadband high frequency (MHz) ultrasound in air and other gases [14-17]. Small variations in density and acoustic velocity are produced in gases by changes in temperature, and hence are ideal for imaging along with flow velocity fields using ultrasonic transmission tomography if suitable transducers are available.

The work to presented here will investigate ultrasonic tomographic imaging of the spatial variation in temperature and flow velocity in gases, using ultrasonic transducers based on an electrostatic principle arranged in a fan-beam geometry. A Fourier transform method based on a filtered back-projection reconstruction algorithm, with rebinning occluded data compensation, will be implemented in LabVIEW® and will also be used to investigate the effect of different Kernel functions on the reconstructed images.

II FAN-BEAM GEOMETRY

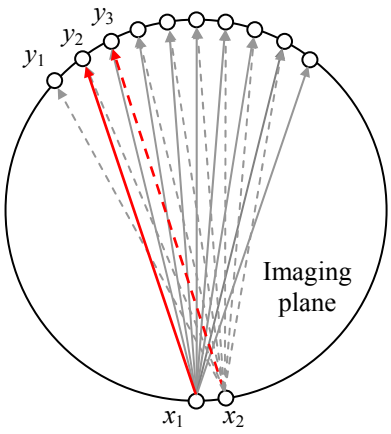

Figure 1: Fan-beam sampling geometry.

A typical fan-beam sampling geometry is shown in Figure 1. A divergent source x_1 producing a wide beam of ultrasound is positioned at the periphery of the area of interest. A receiver y is moved through a series of regularly spaced positions $y_1, y_2, \ldots y_n$ opposite the source, to produce a fan-shaped set of rays known as a *projection*. The source is then moved to new positions $x_2, x_3, \ldots x_n$ in regular steps and the process repeated, so that a whole series of projections at different angles through the scanned area is obtained. A property of each ray in each projection is measured and passed into the tomographic reconstruction algorithm. This is usually propagation time, but may also be amplitude or frequency content.

For any ray path between a transmitter x and receiver y, both the local speed of sound and the gas flow velocity will have an effect on the propagation time t_{xy}, given by:

$$t_{xy} = \int_{r_x}^{r_y} \frac{1}{c_r + \underline{\mathbf{v}} \cdot \hat{\mathbf{r}}} dr \qquad (1)$$

where c_r is the speed of sound at any position r along the ray path, $\underline{\mathbf{v}}$ is the local flow velocity of the gas and $\hat{\mathbf{r}}$ is a unit vector parallel with the ray path and pointing in the direction of integration. For ultrasound propagating in air, the local sound speed c_r is also related to air temperature T in Kelvin by [18]:

$$c_r = 331.31\sqrt{\frac{T}{273.16}} \qquad (2)$$

and so a reconstructed image of the spatial variation in slowness within the scanned area will indicate the presence of solid objects, air flows, or changes in air temperature. Further details of this temperature and flow reconstruction technique can be found in earlier work on parallel beam tomography in gases by Wright *et al* [13].

III FILTERED BACK PROJECTION ALGORITHM

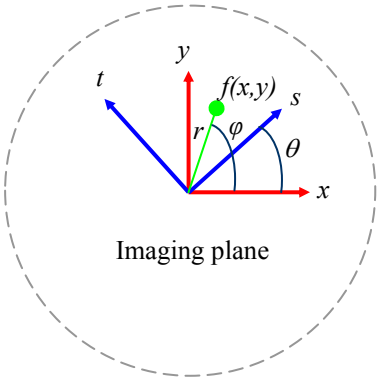

Figure 2: The rotated coordinate system.

Let $f(x,y)$ be the spatial distribution of acoustic slowness (the slowness function) in the area to be scanned [1,11]. The (x,y) coordinate system rotated through any angle θ is denoted (s,t), where:

$$\begin{aligned} s &= x\cos\theta + y\sin\theta \\ t &= -x\sin\theta + y\cos\theta \end{aligned} \qquad (3)$$

as shown in Figure 2.

The projection $p_\theta(s)$ of the slowness function $f_\theta(s,t)$ at an angle θ through the region is given by:

$$p_\theta(s) = \int_{-\infty}^{\infty} f_\theta(s,t).dt \qquad (4)$$

and its Fourier transform $P(S)$ by:

$$P_\theta(S) = \int_{-\infty}^{\infty} p_\theta(s).e^{-j2\pi sS} ds \qquad (5)$$

Hence:

$$P_\theta(S) = \int_{-\infty-\infty}^{\infty\infty} f_\theta(s,t).e^{-j2\pi sS} ds.dt \qquad (6)$$

The Fourier transform $F_\theta(S,T)$ of the slowness function $f_\theta(s,t)$ at an angle θ through the region is:

$$F_\theta(S,T) = \int_{-\infty-\infty}^{\infty\infty} f_\theta(s,t).e^{-j2\pi(sS+tT)} ds.dt \qquad (7)$$

When evaluated at $T = 0$ at the centre of the region,

$$F_\theta(S,0) = \int_{-\infty-\infty}^{\infty\infty} f_\theta(s,t).e^{-j2\pi(sS)} ds.dt \qquad (8)$$

which is simply the transform of the projection in equation (6). Hence:

$$P_\theta(S) = F_\theta(S,0) = F(S\cos\theta, S\sin\theta) \qquad (9)$$

Thus the projection theorem states that the 1-dimensional Fourier transform of a *projection* of the slowness function at any angle θ is equivalent to the 2-dimensional Fourier transform of the *actual* slowness function at the same angle θ, but through the centre of the scanned region.

The slowness function *f(x,y)* may be found at any point from the inverse Fourier transform:

$$f(x,y) = \int_{-\infty}^{\infty}\int_{-\infty}^{\infty} F(X,Y)e^{j2\pi(xX+yY)}dXdY \quad (10)$$

Using polar coordinates:

$$\begin{aligned} x &= r\cos\varphi \\ y &= r\sin\varphi \end{aligned} \quad (11)$$

in the spatial domain and:

$$\begin{aligned} X &= R\cos\theta \\ Y &= R\sin\theta \end{aligned} \quad (12)$$

in the Fourier domain, and:

$$\cos(\theta-\varphi) = \cos\theta\cos\varphi + \sin\theta\sin\varphi \quad (13)$$

equation (10) reduces to:

$$f(x,y) = \int_{0}^{\pi}\int_{-\infty}^{+\infty} F(R\cos\theta, R\sin\theta)e^{j2\pi rR\cos(\theta-\varphi)}|R|dRd\theta \quad (14)$$

where:

$$|R|dRd\theta = dXdY \quad (15)$$

By substituting the transform of the projection $P_\theta(R)$ for the slowness function $F(R\cos\theta, R\sin\theta)$, and introducing a new variable $r' = r\cos(\theta - \varphi)$ equation (14) reduces to:

$$f(x = r\cos\varphi, y = r\sin\varphi) = \int_{0}^{\pi} d\theta \int_{-\infty}^{+\infty} dR|R|P_\theta(R)e^{j2\pi Rr'} \quad (16)$$

The inner integral in equation (16) is simply a convolution in the Fourier domain of the projection $p_\theta(r)$ with a kernel function $k(r)$ whose Fourier transform is $|R|$. By defining a new function $g_\theta(r)$ which is the result of this convolution, given by:

$$g_\theta(r) = p_\theta(r) * k(r) \quad (17)$$

and:

$$G_\theta(R) = P_\theta(R)|R| \quad (18)$$

Equation (16) finally reduces to:

$$\begin{aligned} f(x,y) &= \int_{0}^{\pi} g_\theta(r')d\theta \\ f(x = r\cos\varphi, y = r\sin\varphi) &= \int_{0}^{\pi} g_\theta(r\cos[\theta-\varphi])d\theta \end{aligned} \quad (19)$$

This is just a simple backprojection of all the convolved projections $g_\theta(r')$ associated with all the rays passing through $(x = r\cos\varphi, y = r\sin\varphi)$. Therefore the slowness function may be obtained by convolving all the projections with a kernel function, which is a filtering operation in the Fourier domain.

IV THE KERNEL FUNCTION

As the data consists of *m* projections at regular angular intervals, each containing *n* rays regularly spaced at intervals of Δs, Riemann approximations to the integrals may be used. Due to the discrete sampling period Δs in each projection, the convolutions will be bandwidth limited by the Nyquist theorem to a cut-off frequency of $B = 1/(2\Delta s)$. To prevent aliasing, the ray spacing must be $\Delta s \le 1/(2s_0)$, where s_0 is the highest spatial frequency of interest.

The kernel function must therefore be zeroed above the cut-off frequency, leading to high frequency oscillations in the reconstruction when the ideal Ram-Lak kernel function $|R|$ is used. Therefore an additional windowing function is often used to suppress this high frequency noise by reducing the step at the cut-off frequency. There are a number of different kernel filter functions that may be used in the filtered back projection reconstruction algorithm, with a selection shown in Figure 3:

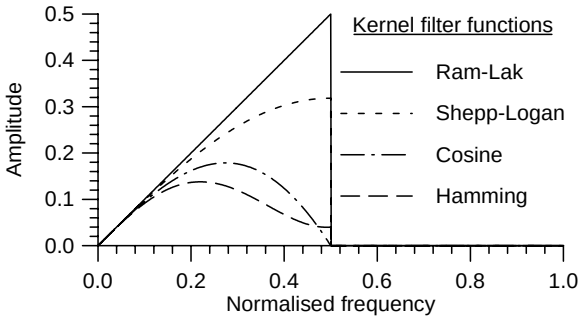

Figure3: Typical Kernel filter functions.

The basic Ram-Lak function $|R|$ is windowed to give the Shepp-Logan kernel function:

$$\frac{2B}{\pi}\left|\sin\left(\frac{2\pi R}{B}\right)\right| \quad (20)$$

the Cosine kernel function:

$$|R|\cos\left(\frac{2\pi R}{B}\right) \quad (21)$$

and the Hamming kernel function:

$$|R|\left\{\alpha + (1-\alpha)\cos\left(\frac{\pi R}{B}\right)\right\} \quad (22)$$

usually with the roll-off $\alpha = 0{\cdot}54$.

The selection of the kernel filter function can therefore have a significant effect on the quality of the reconstructed image, depending on the magnitude of the variations in acoustic slowness in the imaging plane. Where there are large discontinuities in slowness, for example in the tomographic imaging of solid objects in air, the low frequencies in the transformed projections in the Fourier domain will be reduced and the high frequencies emphasised by the basic Ram-Lak and Shepp-Logan filters, introducing noise into the reconstruction. Where only slight variations in acoustic slowness exist, for example in the tomographic imaging of temperature distributions or flow velocity fields, the necessary high frequencies

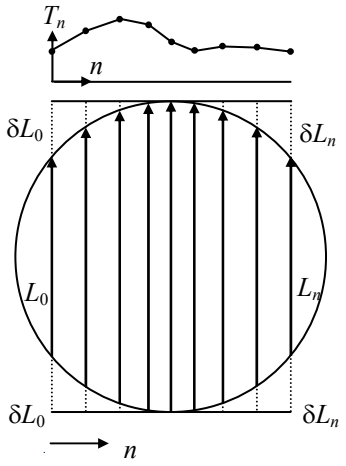

Figure 4: Re-binning the parallel rays.

will be reduced by filters such as the Cosine and Hamming. For general reconstructions, filters that emphasises the mid-range of frequencies will be most appropriate. Some prior knowledge of the expected slowness variations is therefore advantageous.

V RE-BINNING FAN-BEAM DATA

The filtered back-projection algorithm requires projections of regularly spaced parallel rays of equal length. These can be obtained from projections of fan-beam rays using a process known as re-binning [12].

In multiple fan-beam projections, certain rays in different projections will be parallel to each other, e.g. rays x_1y_2 and x_2y_3 in Figure 1. All the parallel rays from different fan-beam projections may be grouped together to form projections of parallel rays of unequal length and irregular spacing, as shown schematically in Figure 4. The ray spacing is equalised by a simple linear interpolation between adjacent values in the projection. The length of each ray is extended by extrapolating by δL_n as required, assuming that the acoustic slowness along the raypath outside the scan area is identical to the background slowness value within the scanned region, increasing the total propagation time from t_n to T_n for each ray according to:

$$T_n = \left(\frac{2\delta L_n}{c_{ref}} \right) + t_n \qquad (23)$$

where c_{ref} is obtained from the first ray (L_0, t_0). The re-binned projections may then be used in the standard parallel beam filtered back projection reconstruction algorithm.

VI EXPERIMENT

In order to maximise the number of rays in each projection, a divergent source and receiver are required, as can be seen from Figure 1. A pair of novel curved electrostatic ultrasonic transducers was employed for both generation and detection of ultrasound in air. They consisted of polished convex metal backplates with a 10 mm radius of curvature and 5μm thick metallised PET dielectric film, and operated at a centre frequency of 400 kHz with a -6dB bandwidth of 300 kHz. The basic operation of electrostatic transducers has been described elsewhere [14-16].

The experimental configuration is shown schematically in Figure 5. The source transducer was driven by a Panametrics Pulser-Receiver (Model 500PR) that delivered a negative spike of up to -250 V with a pulse energy of up to 19.4μJ, and biased using a 100V dc supply. The receiver was connected to a Cooknell SU2/C power supply that provided a dc bias of 100V, and to a Cooknell CA6/C charge amplifier with a sensitivity of 250 mV/pC. Each transducer was mounted on a rotary stage driven using a stepper motor under RS-232 control with a resolution of ±0.02°. The received waveforms were then digitised on a Tektronix TDS224 oscilloscope and transferred to a PC via a RS-232 interface for storage and analysis.

Each tomographic scan consisted of 37 receiver positions at 5º intervals opposite the source, and 72 source locations in 360º. Not all of this data

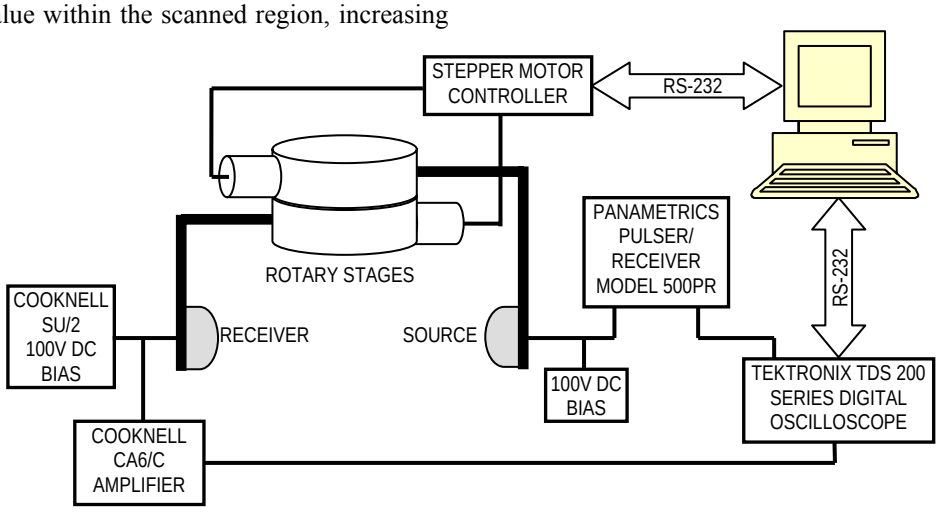

Figure 5: Schematic diagram of experimental apparatus.

was required for the re-bin routine, but it was necessary to ensure that all of the required parallel ray paths were collected. The data acquisition and transducer positioning processes were automated, using routines written in LabVIEW® and RS-232 interfaces. Each waveform was acquired in approximately 10 seconds.

VII RESULTS AND DISCUSSION

Due to the large volume of generated data, only a brief selection of images can be shown here. Figures 6(a) and 6(b) show the reconstructed images of acoustic velocity (reciprocal of slowness) in the scan area with the centre of a 38 mm diameter aluminium cylinder located at the coordinates (0,-10) mm, for the Ram-Lak and Hamming kernel filter functions. As no waveform could be measured travelling directly through the cylinder, there were no propagation times associated with occluded raypaths. A threshold amplitude was therefore employed on the sampled data, with a user-defined propagation time delay inserted to replace the occluded rays. Hence the speed of sound within the object region is entirely artificial. It can be seen that the Ram-Lak filter emphasises the high frequency noise introduced into the reconstruction by the use of occluded data and diffraction around the object. The Hamming filter is more appropriate for imaging the distribution of solid objects as the higher frequencies are suppressed.

In order to image the spatial distribution of temperature, a 6 mm diameter heat source at a constant temperature of 573 K was held centrally below the scanning plane. Reconstructed slowness values were converted into spatial variations in temperature using equation (2) and a typical image is shown in Figure 7, with the heat plume clearly visible in the centre of the image. The background air temperature reconstructed from the tomographic data was between 4% and 7% of the actual air temperature measured using a 1 mm diameter K-type thermocouple. The temperature directly above the heat source was reconstructed to be within 9% of the measured value of 362 K at the height of the scanning plane. The physical size of the transducers meant that considerable spatial averaging occurred to the signals passing through the scan area, which would affect the accuracy of the reconstruction. The background air temperature also fluctuated by ±5 K during the data collection, which means that the temperatures would be time averaged. As a difference technique based on the first ray of the first projection was used, any variations in ambient temperature after this initial acquisition would also affect the reconstruction. The Cosine filter appeared to give the best compromise between image detail and noise in the reconstruction.

Finally, Figure 8 shows a typical reconstruction using the Shepp-Logan kernel function of the flow profile above a 2.7 mm diameter nozzle connected to a compressed air source with a flow rate of 0·5 litres/second measured using a Platon A10HS flowmeter. This figure shows the additional horizontal components of the flow velocity of the air jet, reconstructed from slowness data using a value of 347 ms^{-1} for c_r in Equation (1). The maximum additional horizontal component of the flow is shown to be 8.6 ms^{-1} at the centre of the scan area, which is in good agreement with theory. As the turbulence from the nozzle is rapidly fluctuating, the velocities are effectively time averaged over the data acquisition period and the Hamming or Cosine filters may give more realistic results. However, for faster acquisition times, more of the turbulent detail would be included in the image, and the Ram-Lak or Shepp-Logan filter would then be more appropriate. The information reconstructed within the scan area is still limited by the same constraints concerning transducer size, turbulence, time-averaging, compressibility and ray bending.

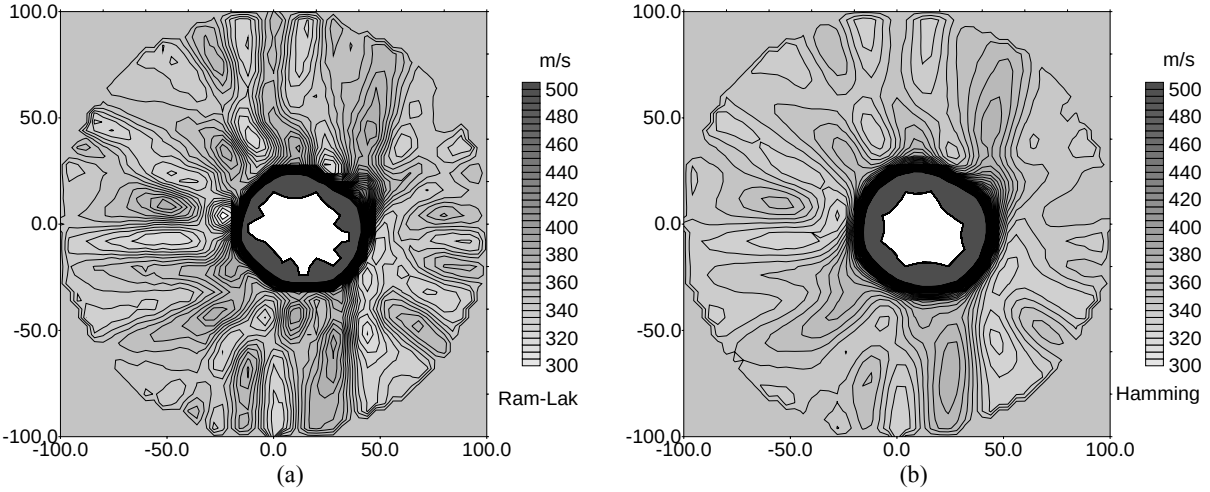

Figure 6: Reconstructions of solid distribution (inverse slowness function).

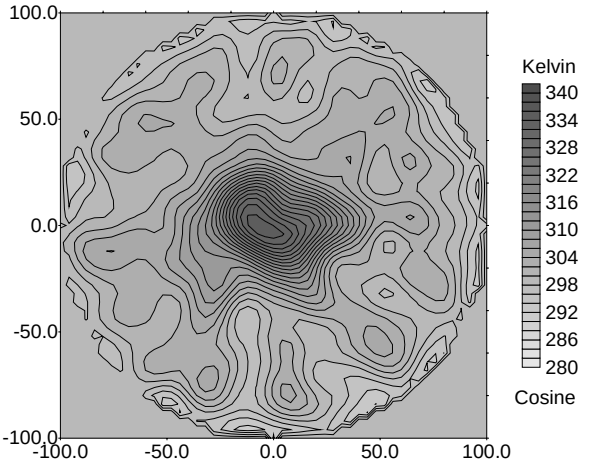

Figure 7: Reconstruction of temperature.

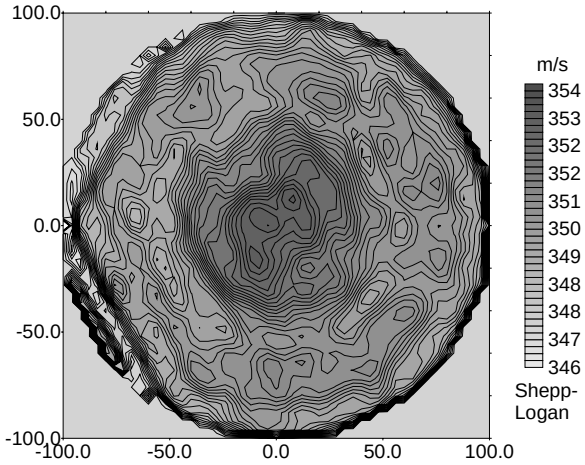

Figure 8: Reconstruction of flow velocity.

VIII CONCLUSIONS

The effect of kernel filter function on the tomographic reconstruction of ultrasonic images in air has been investigated. Using an imaging system consisting of a pair of novel curved electrostatic ultrasonic transducers under computer control and a filtered back-projection algorithm, images of solid object distribution, temperature variation and flow velocity in air were produced. The Hamming filter function that suppressed high frequencies was most suitable for solid object distribution, and the Cosine filter was most suitable for detailed temperature distributions. The filter choice for flow velocity imaging was determined by the level of detail required, with the Shepp-Logan filter function giving the best compromise.

IX ACKNOWLEDGEMENTS

This work was supported by a Marie Curie Research Fellowship no. HPMF-CT-1999-00038.

X REFERENCES

[1] A.C. Kak and M. Slaney, *Principles of Computerized Tomographic Imaging*, IEEE Press, New York, (1988)

[2] H. W. Jones, 'Recent activity in ultrasonic tomography', *Ultrasonics*, Vol. 31, No. 5, pp. 353-360 (1993)

[3] L. Capineri, H.G. Tattersall, J. A. G. Temple and M. G. Silk, 'Time-of-flight diffraction tomography for NDT applications', *Ultrasonics*, Vol. 30, No. 5, pp. 275-288 (1992)

[4] K. A. Dines and S. A. Goss, 'Computed Ultrasonic Reflection Tomography', *IEEE Trans. Ultrason. Ferroelec. Freq. Contr.*, Vol. UFFC-34, No. 3, pp. 309-318 (1987)

[5] A. M. H. Satti and J. Szilard, 'Computerized ultrasonic tomography for testing solid propellant rocket motors', *Ultrasonics*, Vol. 21, pp. 162-166 (1983)

[6] O. M.Warsito, N. Kawata and S. Uchida, 'Cross-sectional distributions of gas and solid holdups in slurry bubble column investigated by ultrasonic computed tomography', *Chemical Engineering Science,* Vol. 54, No. 21, pp. 4711-4728 (1999)

[7] G. J. Brown and D. Reilly, 'Ultrasonic tomographic imaging of solid objects in air using an array of fan-shaped-beam electrostatic transducers', *Ultrasonics,* Vol. 34, pp. 111-115 (1996)

[8] J. Greenleaf, S. Johnson, W. Wamoya and F. Duck, 'Algebraic reconstruction of spatial distributions of acoustic velocities in tissue from their time-of-flight profiles', *Acoust. Hologr.*, Vol. 6, pp. 71-90 (1975)

[9] R. Gordon, R. Bender and G. T. Hermann, 'Algebraic reconstruction techniques for three-dimensional electron microscopy and X-ray photography', *J. Theor. Biol.*, Vol. 29, pp. 471-481 (1970)

[10] Y. Censor, 'Finite Series-Expansion Reconstruction Techniques', *Proc. IEEE*, Vol. 71, pp. 409-419 (1984)

[11] A. J. Devaney, 'Fast Filtered Backpropagation Algorithm for Ultrasound Tomography', *IEEE Trans. Ultrason. Ferroelec. Frequ. Contr.*, Vol. UFFC-34, pp. 330-340 (1987)

[12] T. M. Peters and R. M. Lewitt, 'Computed tomography with fan-beam geometry', *J. Comput. Assist. Tomog*., Vol. 1, pp. 429- (1977)

[13] W. M. Wright, D. W. Schindel, D. A. Hutchins, P. W. Carpenter and D. P. Jansen, 'Ultrasonic Tomographic Imaging of Temperature and Flow Fields in gases using Air-Coupled Capacitance Transducers', *J. Acoust. Soc. Am.,* Vol. 104, pp.3446-3455 (1998)

[14] H. Carr and C. Wykes, 'Diagnostic Measurements in Capacitive Transducers', *Ultrasonics*, Vol. 31, pp. 13-20 (1993)

[15] D. Schindel, D. Hutchins, L. Zou and M. Sayer, 'The Design and Characterization of Micromachined Air-Coupled Capacitance Transducers', *IEEE Trans. Ultrason. Ferroelec. Frequ. Contr.*, Vol. UFFC-42, pp. 42-50 (1995)

[16] M. Oksanen, J. Varis, J. Hietanen and J. Wu, 'Quantitative theory for V-groove capacitive transmitting transducers', *Ultrasonics,* Vol. 35, pp. 205-211 (1997)

[17] B. Khuri-Yakub, F. Degertekin, X. Jin, S. Calmes, I. Ladabaum, S. Hansen, X. Zhang, 'Silicon micromachined ultrasonic transducers', *Proc. IEEE Ultrasonics Symposium*, Vol. 2, pp. 985-991 (1998)

[18] R. Hickling and S. P. Marin, 'The Use of Ultrasound for Gauging and Proximity Sensing in Air', *J. Acoust. Soc. Am.* Vol. 79, pp. 1151-1160 (1986)